Surfaces and Interfaces 23 (2021) 100922

Contents lists available at ScienceDirect

Surfaces and Interfaces

journal homepage: www.sciencedirect.com/journal/surfaces-and-interfaces

Confined hydration in nanometer-graded plasma polymer films: Insights from surface-enhanced infrared absorption spectroscopy

Ezgi Bülbül [a,b], Dirk Hegemann [a,*], Kenichi Ataka [c], Sandro Lehner [a], Joachim Heberle [c], Manfred Heuberger [a,b]

[a] Laboratory for Advanced Fibers, Empa, Swiss Federal Laboratories for Materials Science and Technology, St. Gallen, 9014, Switzerland
[b] Laboratory for Surface Science and Technology, Department of Materials, ETH Zurich, Zurich, 8093, Switzerland
[c] Department of Experimental Molecular Biophysics, Freie Universität Berlin, Berlin, 14195, Germany

ARTICLE INFO

Keywords:
Siloxane plasma polymers
Amphiphilic gradient
Subsurface hydration
Water confinement

ABSTRACT

To shed light on recently explored long-range surface forces generated by subsurface-confined water, the structural characteristics of water molecules penetrating into nanoporous homogeneous and nanograded siloxane plasma polymer films (PPFs) over the time scale of 24 hours are studied by surface-enhanced IR spectroscopy (SEIRAS). Chemically graded PPFs, with embedded hydrophobic-to-hydrophilic gradient, are found to significantly change the average interfacial water orientation due to a unique nanoporous morphology and silanol group coordination. Diffusion of water through the hydrophobic SiO:CH matrix creates an evolution of the coordination of matrix silanol groups, which are eventually deprotonated as soon as the hydration network connects to the aqueous environment. This occurs after ~6 hours of water immersion and coincides with the change of average interfacial water orientation. Both effects are present on hydrophobic samples, but are significantly amplified by the presence of the subsurface vertical amphiphilic gradient (Vgrad), whereas enhanced water uptake in oxygen-plasma modified graded PPFs is covering such effects.

Introduction

Water, being the most important solvent, exhibits remarkably multifaceted properties owing to a triple balance of interactions involving a significant dipole moment, substantial polarizability as well as a tetragonal hydrogen bonding capability [1,2]. It is known that local ordering and molecular dynamics change in distinguished ways when water is confined to nanosized cavities. An often discussed alteration is the locally modified hydrogen-bond network [3–6]. Confined water has consequently attracted a considerable amount of attention, not the least since it plays a decisive role in areas ranging from biological processes to nanotechnology, catalysis, and soil chemistry [2,7–10]. The energetic and structural properties of confined water, such as hydrogen bond distribution, clustering, proton mobility, are controlled by confinement geometry as well as the distinguished interaction with the confining surfaces or matrix [11].Among numerous experimental and theoretical research works conducted in recent years, there is a notable interest in understanding the structural and dynamic properties of water confined to matrix-defined channels of different geometry e.g. slit, cylindrical, or disordered networks of pores [12–18].

The occurrence of confined water in plasma polymer films (PPFs) in aqueous environments is of particular technological interest and it has been the focus of recent studies [19–24]. This notably includes PPFs with embedded subsurface amphiphilic gradients that also exhibit a graded transition in porosity. It was found that hydration of such subsurface gradient PPFs leads to modified adsorption of dipolar macromolecules on the surface, suggesting the existence of long-range surface forces, i.e. >10 nm generated by subsurface confined water. It was found that these effects are transient in nature and the evolution encompasses at least 12 hours after being immersed in water for some hours for the examined PPFs [22,24,25]. The here studied plasma polymers are based on siloxane chemistry, e.g. using the established hexamethyldisiloxane (HMDSO) precursor; they are well suited to provide a nanoporous and chemically adjustable matrix [26]. The controlled removal of O_2 admixture from a HMDSO vapor plasma during the film growth conveniently allows the generation of a hydrophilic-to-hydrophobic transition at a chosen depth below the film surface forming a buried interface. Termination of different base layers with the same

* Corresponding author.
E-mail address: dirk.hegemann@empa.ch (D. Hegemann).

https://doi.org/10.1016/j.surfin.2020.100922
Received 6 October 2020; Received in revised form 28 December 2020; Accepted 29 December 2020
Available online 9 January 2021
2468-0230/© 2021 The Authors. Published by Elsevier B.V. This is an open access article under the CC BY-NC-ND license (http://creativecommons.org/licenses/by-nc-nd/4.0/).

hydrophobic surface (SiO:CH) film of nominally 4 nm was used to obtain identical surface chemistry. Optional intermediate plasma oxidation was used to further modify the chemical and morphological composition before the deposition of the SiO:CH terminal layer. Although neutron reflectivity measurements revealed that the time of intermediate plasma oxidation increases the abundance of water in the hydrating subsurface region [22], it remained unclear to what extent such optional oxidation affected the subsurface water-matrix interactions. Within this previous study, the abundance of silanol entities mainly in the hydrophobic and the transition region of the gradient matrix was additionally detected using ToF-SIMS confirming the nanoporous morphology of siloxane PPFs. As it is well-described in the literature, silanol coordinations in the matrix as well as at the surface are of fundamental importance involving interactions with water [27,28]. In contact with water, hydroxylation of siloxane backbones, particularly at the surface as well as at the tip of cracks and pores, is likely to occur addressing the further hydration processes [29,30]. Moreover, hydrogen bonding interaction between silanol and molecular water is known to affect water transport through nanoporous materials [31].

Attenuated total reflection Fourier transform (ATR-FTIR) with a penetration depth around ~1 μm provides a powerful method to obtain structural information on water intruding a thin film matrix or water at an interface. Two prominent features of the aqueous IR spectrum include a bending (1635 cm^{-1}) and a broad stretching band (2800-3700 cm^{-1}) [32–37]. The OH stretching mode is highly sensitive to the strength of water hydrogen bonding with its environment [34,38,39] as indicated by shifts of the peak wavenumber. Ice peaks around ~3220 cm^{-1} [40, 41], and a broad band located around ~3400 $cm^{-1}$is characteristic for bulk water [42]. For the limiting case of non-interacting hydroxyl groups in vapor, a vibrational band appears at ~3640 cm^{-1}. Besides the contribution of different water hydroxyl group vibrations, one component centered around 3200 cm^{-1} of this OH stretching mode is associated with the silanols present in a highly H-coordinated chemical environment [43,44]. Studying the OH stretching band provides a means of investigating the hydrogen bonding interactions of water at aqueous interfaces. The water in close proximity to the surface (<2 nm) often has different properties and is called interfacial water [45]. Rather local properties of the surface control the interfacial water structure, which often remains undetected by more macroscopic surface analytics such as contact angle [28,46]. In the presence of ionic and polar groups on the surface, the adsorbed water molecules can form strongly hydrogen-bonded or ordered structures and can thus be seen in the lower frequency part of the OH stretching band [37,47]. In addition to these well-studied water and silanol vibrations, the relatively weak bending+libration water combination band centered around 2100 cm^{-1} is documented. This band is associated with the H-bond hindered rotation of water molecules, thus reporting on the intermolecular structure and dynamics of liquid water [48–51]. Considering the general scheme of these wavenumber shifts, it can be foreseen that the chemically graded PPF should induce measurable spectral changes in water vibrational modes at the interface and also as water penetrates the matrix [39]. Since we are interested in IR absorption spectra from nanometer thick regions we advance this research effort by means of surface-enhanced infrared spectroscopy (SEIRAS). Several research papers have already reported on the local water structuring characterized by SEIRAS [52–55]. The plasmon resonance of a nanostructured gold film enhances the surface sensitivity, typically one or two orders of magnitude [56–58] as compared to the attenuated total reflection (ATR) approach. The SEIRAS sensitivity decays exponentially [59] with a typical pre-exponent factor of ~$(8\ nm)^{-1}$. Therefore, a predominant portion of the detected IR absorption occurs inside the plasma polymer film, while the signals from interfacial and bulk water above are reduced. Moreover, SEIRAS provides significantly enhanced sensitivity to vibrational modes linked to dipole moments perpendicular to the surface. Owing to these provisions, SEIRAS signal quantification can be challenging. A comprehensive discussion of the underlying EM theory can be found in the literature [57,59–63].

Methods

Plasma polymer deposition

The plasma polymer films (PPFs) were generated in an asymmetric, capacitively coupled reactor. The deposition was performed on the 13.56 MHz radio frequency (RF) driven electrode with an area of 21×70 cm^2, which was mounted inside the reactor vessel with a gap of 8 cm from the chamber wall. A gas showerhead facing the entire electrode area, providing a uniform gas inlet, supplied the gaseous mixture of the monomer hexamethyldisiloxane (HMDSO) (purchased from Fluka), the carrier gas Ar, and the reactive gas oxygen (purchased from Carbagas, Switzerland) into the reactor. The liquid HMDSO was vaporized at reduced pressure and a slightly elevated temperature of 40°C and a thermostabilized mass flow controller (43°C) regulated the gas flow rate of the precursor vapor into the reactor.

A formerly well-defined protocol was employed to deposit two gradient-free reference PPFs and three types of vertical gradient films each with a total thickness of 10 nm at a maintained pressure of 7 Pa [25]. A preceding in-situ cleaning step of the substrate, the gold nanostructured Si-chip, was achieved by Ar/O_2 plasma (80 sccm/20 sccm) with 200 W applied power at 10 Pa pressure. A fixed flow rate of 4 sccm (standard cubic centimeter per minute) of vaporized HMDSO mixed with 20 sccm Ar was fed to generate a 10 nm hydrocarbon-rich (hydrophobic) "SiO:CH" film at a nominal power input of 50 W. The admixture of 40 sccm oxygen to the HMDSO/Ar plasma under a nominal power input of 100 W enabled conditions to produce a 10 nm hydrophilic, hydrocarbon-poor (hydrophilic) "SiOx" film. In an in-situ two--step process, a 6 nm thick SiOx base layer terminated by a nominally 4 nm thick SiO:CH layer together formed the vertical gradient film, entitled "Vgrad".

Optionally, a plasma oxidation step was employed after deposition of the SiOx base layer for 1 min and 5 min, respectively, preceding the deposition of the 4 nm-thick hydrophobic SiO:CH cover layer. These two alternative models of subsurface gradients are named "Vgrad-ox1" and "Vgrad-ox5". The required adjustments in gas flow rates between different conditions could be reliably performed during short periods of plasma power off. A general characterization of the here used PPF with different analytical tools is available in the literature; namely, in terms of film density, elemental composition, stability, water contact angle, and hydration [22,23].

Scanning electron microscopy (SEM)

The impact of the plasma oxidation process on the morphology of SiOx PPFs was investigated by SEM analysis. Thus, a ~6 nm SiOx PPF was deposited on polypropylene films; this thickness ensures full coverage of the polymer substrate. We selected a polymer substrate to contrast coating defects by oxygen species that can undercut the substrate through voids in the SiOx film [64,65] during the optional Ar/O_2 plasma etching (applied for 1 and 5 min, 20/40 sccm, at a power of 100 W).Then, the surface of bare SiOx as well as the oxidized layers were analyzed with SEM (Hitachi S-4800). A ~4 nm thick gold–platinum film was applied onto these non-conducting samples by sputtering before obtaining SEM images.

In-situ surface-enhanced infrared absorption spectroscopy (SEIRAS)

Surface-enhancement is achieved by utilizing a 100-200 nm gold film, which exhibits corrugations of ~50 nm in diameter and a height of 10-20 nm. This gold film was deposited on a silicon chip by chemical deposition [57,58]. Gold was deposited by reduction of hydrogen tetrachloroaurate ($HAuCl_4$) on freshly etched Si surface by exposing diluted HF solution and reductant[57, 58]. Subsequently, one of the five

variants of plasma polymers (SiOx, SiO:CH, Vgrad, Vgrad-ox1, and Vgrad-ox5) was deposited onto the nanostructured gold surface.

The Si chip was finally placed inside a Teflon cell that was mounted in an FTIR spectrometer (Bruker Vertex 70V) equipped with home-built attenuated total reflection optics (single reflection at 60° incident angle). The reflected beam illuminated a mercury cadmium telluride (MCT) detector. A number of 512 scans were recorded for each spectrum with a resolution of 4 cm^{-1}. Hydration of the examined samples is known to proceed over a period of several hours. Therefore, a background spectrum, i.e. quasi dry state, was collected immediately after the injection of 1 mL of distilled water into the sample cell. Afterwards, the IR absorbance spectra of PPF exposed to water was recorded in regular time intervals of 20 min, for a total duration of 24 h. For the data analysis, the background and instrumental water vapor spectra were initially subtracted from each time-resolved SEIRA spectrum and then the baseline was corrected using OPUS 7.2 software. Due to the logarithmic time evolution of the hydration progress, we collected spectra in growing time intervals, namely at 20 min, 1 h, 3 h, 6 h, 10 h, 13 h, 16 h, 20 h, and 24 h of film hydration (see Figure S2 for more details).

The fitting operation of OH stretching bands in the SEIRA spectra, particularly obtained at quasi-dry and 24 h hydrated states, was deconvoluted using a Gaussian peak shape. The assignment of two important sub-bands includes bulk-like water and highly coordinated OH configurations. The latter contains several contributions, since the frequency range for ice-like water and highly coordinated silanol overlap; we were not able to clearly distinguish them during the fitting procedure. Thus, they were considered as one composite peak named "highly coordinated OH".The position, amplitude, and width of this composite peak are thus characteristic of the different hydrogen-bonding environments of each sample. However, bulk-like water, as detected above the interfacial water of the surface, can be observed for all samples. Thus, the location of the bulk-like water peak (3311 cm^{-1}) and its width (384 cm^{-1}) were fixed during Gaussian deconvolution, according to values determined from an independent ATR-FTIR characterization of bulk water.

For the ATR-FTIR characterization of a pure water reference, droplets of nanopure water were directly put onto a GladiATR (Pike Technologies, Fitchburg, USA) which was operated in combination with a Tensor 27 IR-spectrometer (Bruker AG, Fällanden, Switzerland). For the analysis, 32 scans at a resolution of 4 cm^{-1} were recorded between 4000 cm^{-1} and 650 cm^{-1}.

Results and discussion

Fig. 1 schematically illustrates how SEIRAS was set up in a small fluid cell to investigate the hydration of the subsurface-modified siloxane PPFs coated onto a nanostructured Au coating. The vibrational spectra of the two gradient-free reference PPFs, as well as the gradient films, were acquired in form of time series during 24 hours, whereby the recording started immediately (<1 min) after water injection.

Water contact angle (WCA) measurements indicated that the SiOx base layer is moderately hydrophilic (WCA of 72) due to a small fraction

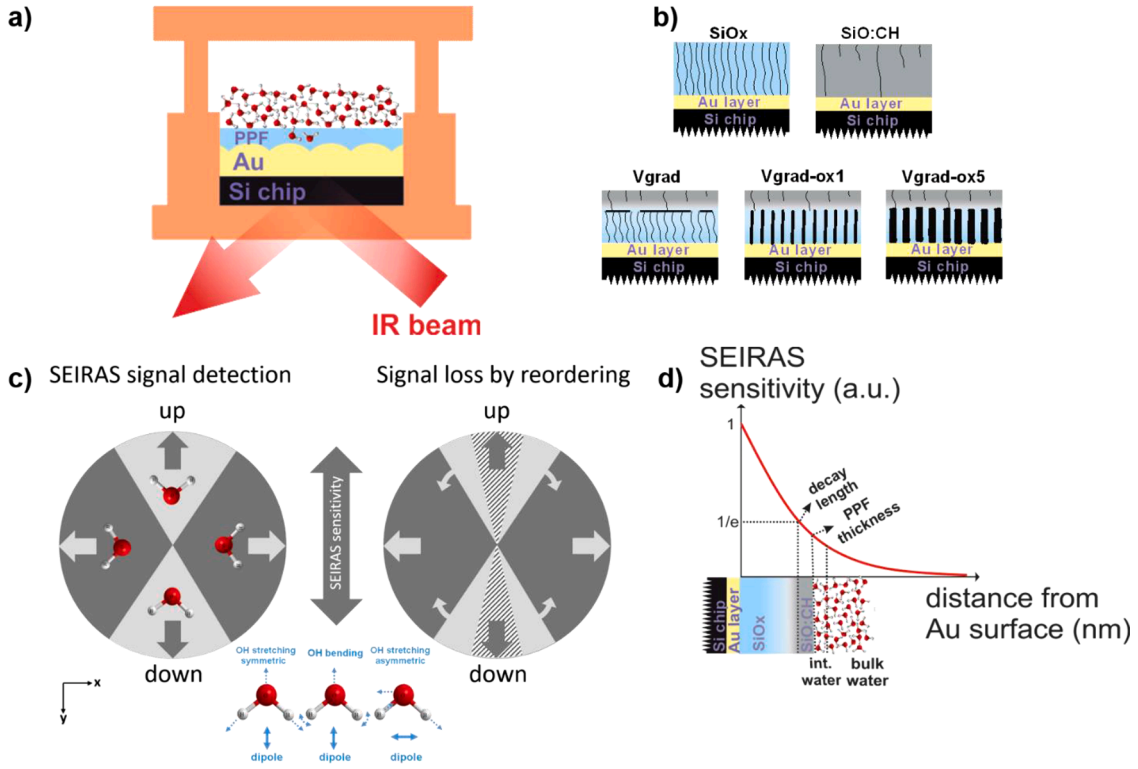

Fig. 1. Schematic illustration of the experimental approach. **a)** The SEIRAS optical cell was filled with 1 mL of distilled water at the start of each hydration experiment using a plasmonic nanostructured gold film coated with different plasma polymer films (PPFs); **b)** Schematic illustration of the examined PPFs under hydration conditions: hydrophilic SiOx film exhibiting nanopores along the granule boundaries; hydrophobic SiO:CH film with more finger-like nanochannels; vertical gradient film (Vgrad) with embedded 1-2 nm wide hydrophilic-to-hydrophobic gradient at the interface of a 6 nm hydrophilic base layer (SiOx) and a 4 nm hydrophobic cover layer (SiO:CH); similar gradient films with additional plasma oxidation step applied for 1 (Vgrad-ox1) and 5 min (Vgrad-ox5) on the 6 nm SiOx base layer; **c)**Schematic representation of the SEIRAS signal that detects only the perpendicular dipole component of OH vibration, i.e. up and down orientation with respect to the surface, as indicated by the light-gray shaded areas, whereas water dipoles oriented in the horizontal plane are not measured. Note that water dipole directions are three dimensional, therefore the SEIRAS signal would detect less than one-third of randomly oriented water molecules. Changes in the average water molecule orientation, as indicated by small arrows, results in corresponding changes of the SEIRAS signal, e.g. smaller light shaded areas.**d)** Sketch of SEIRAS exponential sensitivity characteristics, with a pre-exponential factor of typically ~$(8\ nm)^{-1}$ in relation to the used PPF architectures of nominally 10 nm thickness. Interfacial and bulk water OH vibrations are thus probed at lower sensitivity compared to OH vibrations occurring in the PPF matrix.

of incorporated hydrocarbons, whereas the nominally 4 nm thick terminating SiO:CH layer is hydrophobic (WCA of 105°). Depositing these two film types in sequence, an interface with a vertical chemical gradient named "Vgrad" is formed (see Fig. 1b). Additional plasma oxidation of the SiOx base layer, with a duration of 1 or 5 min, was applied for the samples named Vgrad-ox1 and Vgrad-ox5 (see Fig. 1b), respectively, thereby strongly reducing the ex-situ measurable WCA [22]. From previous results, we expect samples Vgrad-ox1 and Vgrad-ox5 to exhibit a different embedded nanopore morphology due to the etching of the residual hydrocarbons, as sketched in Fig. 1b and also imaged in Fig. 4.All gradient samples are fully covered by the hydrophobic SiO:CH termination layer, thus exhibiting identical surface wetting properties with a WCA of 105°. Furthermore, the surface roughness (~0.3 nm), as well as the essentially PDMS-like chemical composition of the termination layer, are identical to the 10 nm thick gradient-free SiO:CH reference film (as observed from AFM and ToF-SIMS, not shown). However, such PPFs can contain other terminal groups like Si-H, and Si-OH besides Si-CH_3, typically considered as defects [21,66]. A varying amount of silanol groups was previously detected in the examined PPF variants using ToF-SIMS, confirming the adjustable density of chemically unconnected local network branches in the plasma polymer matrix indicative of nanoporosity [20,22].

Changes in the SEIRA OH vibrational spectrum of water molecules and the matrix were recorded for 24 hours. An independent quantification of D_2O penetration into such PPFs is available from neutron reflectivity measurements taken at comparable hydration times [22,23,67]. Note that SEIRAS selectively detects vibrational modes where the dipole component is perpendicular to the surface [57,63], implying that both OH stretching and OH bending modes of water are selectively detected for molecules that are oriented normal to the surface, as illustrated in Fig. 1c. Due to an exponentially decaying sensitivity, SEIRAS is more sensitive to molecular vibrations in the PPF matrix, yet the SEIRAS signal still contains significant contributions from interfacial as well as bulk water above the PPF surface (Fig. 1d). While the OH bending region is purely associated with water, the OH stretching region results from a superposition of matrix silanol (Si-OH) as well as water OH, in the different local environments. Table 1 names different known H-bonding environments and associated typical wavenumbers, i.e. bulk-like water [42], ice-like water [40,41], and highly coordinated silanol [43,44,68]. Due to a significant frequency overlap and shifting, the identification of individual contributions is difficult and quantification by spectral deconvolution is furthermore complicated by the highly non-linear sensitivity. Qualitatively nonetheless, there is a general trend that OH stretch vibrations exhibit lower wavenumbers with increasing hydrogen bond coordination [69]. Note that the opposite trend is documented for the OH bending band [70]. Along these lines, ice-like water vibrations were previously assigned to ordered interfacial water [32]. Highly coordinated silanol groups can occur inside the dry PPF matrix and contribute to the same OH stretching band. A high degree of coordination occurs if two adjacent silanol groups form hydrogen bonds. The literature specifies a critical distance for high inter-silanol coordination of 3.3 Å [31,71,72]. Most of the silanols in the PPF must be highly coordinated to explain the here observed IR signal centered around 3150 cm^{-1}. HMDSO-based PPFs contain a controllable amount of (Si-OH)-O-(Si-OH) sequences in the matrix [73], which favor such inter-silanol coordination. The inset in Table 1 summarizes the different vibrational frequency ranges, which can be assigned to the main features seen in the here analyzed SEIRA spectra.

The SEIRA spectra of the five different PPFs are shown in Fig. 2a and b, at the start of hydration (i.e. <1 min after injection) and after 24 h of hydration, respectively. Due to the spectral overlap of several contributions and the exponentially decaying sensitivity of SEIRAS, a direct

Table 1
List of the evaluated OH symmetric stretch vibrations and their assignments.

Type of hydroxyl network	Infrared hydroxyl stretching region
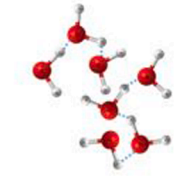 **Bulk-like water** (Constant breaking and forming of H-bonds)	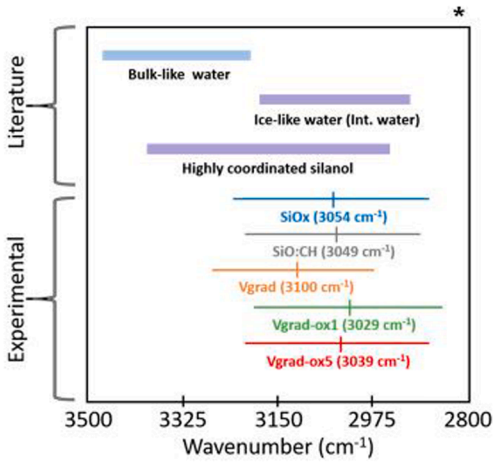
Ice-like water (Stable H-bonds)	
Highly coordinated silanol (Coordination increases with lowering the distance between silanols)	

*The inserted figure represents the IR frequency range of bulk water (light blue), ice-like water (purple) and highly coordinated silanol (purple), accessed from the literature. Besides, the highly coordinated OH band (a combination of ice-like water and highly coordinated silanol) as obtained from the peak fitting are shown as bars centered at 3054, 3049, 3100, 3029, and 3039 cm^{-1} for SiOx (blue), SiO:CH (gray), Vgrad (orange), Vgrad-ox1 (green), and Vgrad-ox5 (red), respectively, where the length of the bar corresponds to the full-width half maximum of the peak.

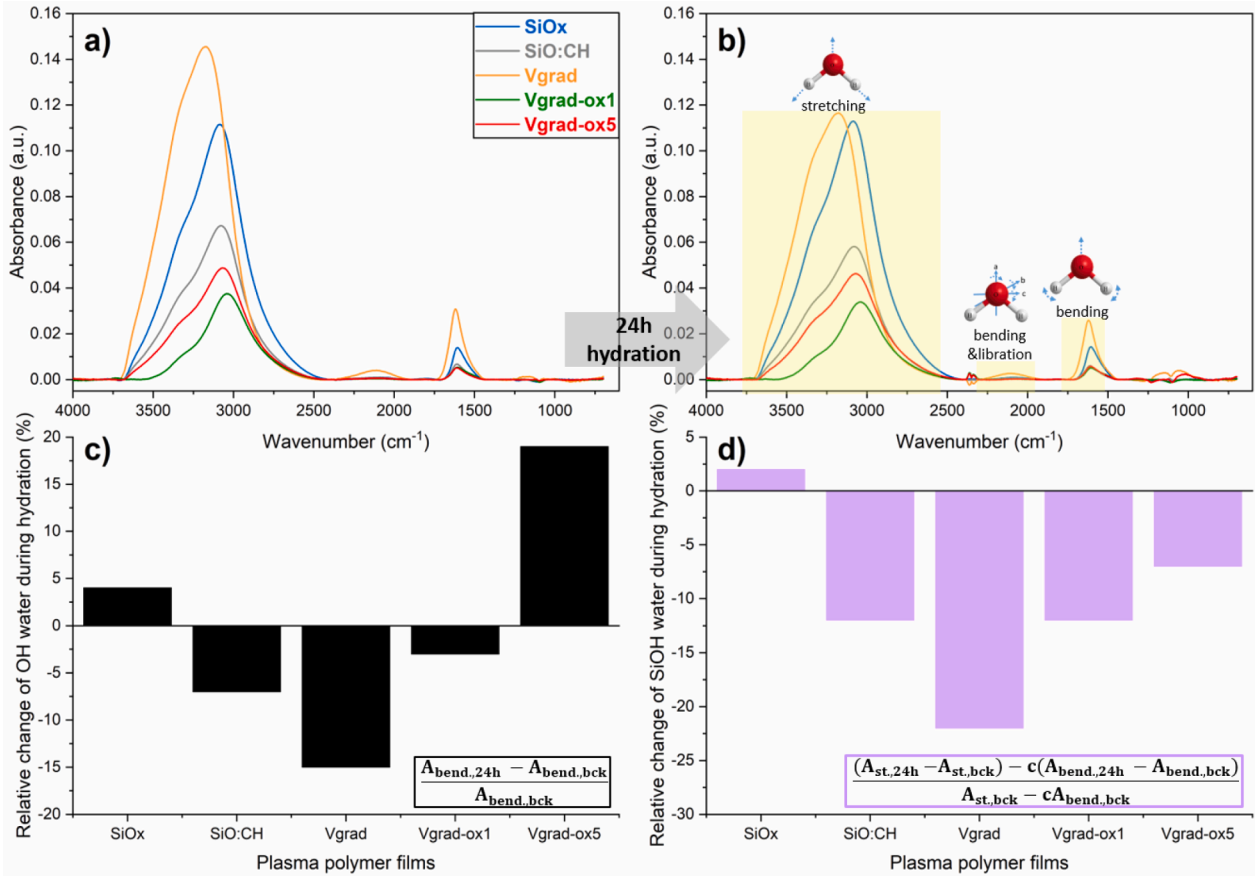

Fig. 2. SEIRA spectra recorded during 24 h hydration series. **a)** hydration start measured <1min after water injection (SiOx - blue curve, SiO:CH - gray curve, Vgrad - orange curve, Vgrad-ox1 - green curve, Vgrad-ox5 - red curve); a polynomial baseline with identical fixpoints at hand-selected wavenumbers was subtracted from all spectra (Fig. S1); **b)** after 24 h of hydration with identification of OH stretching band, bending+libration combination band and OH bending band; the same polynomial fixpoints were used for baseline subtraction as above; **c)** relative integral area changes occurring in the bending region during 24 h hydration, this ratio highlights relative changes occurring in the amount of water with a surface-normal orientation, i.e. interfacial and matrix-confined water; **d)** the estimated relative change of matrix Si-OH signal during 24 h hydration estimated from an integral area difference analysis; the constant factor, c ≈ 9.6, estimates the constant stretching-to-bending-area-ratio from an independent ATR-FTIR measurement with a drop of millipore water (Fig. S3).

spectral quantification via deconvolution of the IR spectra is not workable. Instead, one can use integral area arguments to obtain a semi-quantitative insight into the changes occurring during the 24 h hydration. To analyze the more complex stretching band (~3000-3400 cm^{-1}), we shall make use of the particulars that i) the bending region (~1635 cm^{-1}) solely consists of water contributions (i.e. no silanol), and ii) the fixed relationship between the integral areas of stretching-to-bending signal for water, as verified from independent ATR-FTIR measurements.

The relative changes of the integral area in the bending region are displayed in Fig. 2c. Notably, some of the samples exhibit a negative change of IR absorption, despite the fact that previous NR results detected intrusion of 10-15 vol% D_2O during the same time period [22, 23]. The expected increase of signal due to water intrusion must be masked by a larger loss of signal due to water dissociation or water reorientation. A modified water dissociation in nanopores was proposed by other groups [74,75], but this is unlikely to explain the observation since the invisibility of water intrusion in nanopores does not result in a relative loss of the SEIRAS signal. Hence, the observed negative change needs to be related to the reordering of vertically oriented interfacial water during the hydration process (Fig. 1c). It is difficult to quantify the exact amount of reoriented water, but, if the water that penetrates the matrix is largely invisible, it must contribute equal or more than -15% (observed decrease in Vgrad, Fig. 2c) to the initial OH vibration band. The signal loss of the initially vertically orientated portion of the water is pronounced for the Vgrad architecture, which was previously found to exhibit unusually reduced adsorption of BSA on the surface [22–25]. Along these lines, reordering of interfacial water is also seen in the SEIRAS signal of the reference hydrophobic (SiO:CH) layer; the latter also exhibits lower protein adsorption compared to the SiOx reference surface [22], which shows no noticeable water reordering. One might expect a certain amount of reoriented water on all four samples that are terminated by the same hydrophobic SiO:CH layer. The reduction of the water signal is less pronounced for Vgrad-ox1, and Vgrad-ox5 is even dominated by a clear increase of signal. Both findings agree with the observed higher amount of water intrusion, which can mask water reorientation effects. Increased amounts of D_2O diffusing into this type of PPF was previously also seen in NR, in the same order of oxidation duration [22]. These fundamental differences of the oxygen treated samples concur with the different protein adsorption reported earlier; namely, the Vgrad-ox5 was found not to show the related decrease in protein adsorption [22].Last but not least, the hydrophilic PPF (SiOx) shows only a small increase (~5 %) of water signal during hydration, which suggests that interfacial reorientation is less significant here.

To obtain an estimation for the relative change of silanol groups in the matrix from SEIRAS data, we determined the constant area ratio factor, $c = \int I(\text{stretching})\, dA \,/\, \int I(\text{bending})\, dA \approx 9.6$, of a bulk water ATR-FTIR reference spectrum (Fig. S3). Multiplying the integral area of the SEIRAS bending region by this factor, c then allows subtraction of the water contribution from the stretching band and henceforth isolates the matrix silanol part. The underlying assumption that the orientation of silanol groups in the PPF is essentially random, seems plausible. As seen in Fig. 2d, the SiOx sample exhibits a small increase of silanol

absorption during hydration. Initially, SiOx contains a negligible amount of Si-OH [22]. Silanols, however, can be formed upon water intrusion by the chemical equilibrium reaction Si-O-Si + H_2O ↔ (SiOH)-(SiOH) along pore surfaces and boundaries between adjacent amorphous SiOx granules[30,76]. The more hydrophobic SiO:CH matrix contains trapped radicals after plasma deposition that react with humidity to Si-OH, which probably forms nanochannels along with such defective spots [20]. Along such nanochannels the embedded coordinated Si-OH groups can slowly deprotonate upon water intrusion; SiOH + H_2O ↔SiO^- + H_3O^+[27,28]. The silanol deprotonation reaction occurs in all samples with SiO:CH composition and leads to a loss of signal during hydration. This effect is strongest for the Vgrad sample, yet also visible for the Vgrad-ox1 and Vgrad-ox5 variants in decreasing order.

To shed light on the time evolution and the interactions between water and matrix, we shall perform a detailed differential spectral analysis below. Therefore, we subtracted the first spectrum measured at hydration start (<1 min after water injection) from all subsequently measured spectra (see Figure S2). The hence obtained difference spectra series is displayed in Fig. 3. Note that the light orange line in Fig. 3 marks the constant location of the CO_2 absorptioncaused in the experimental surroundings. Furthermore, the wavenumbers for bulk water (~3400 cm^{-1}) and highly coordinated OH (~3000-3200 cm^{-1}) are also marked with light blue and purple lines for convenience.

The plain reference films consisting of SiOx and SiO:CH both exhibit an initial increase of signal in the composite stretching band 3600 to 3000 cm^{-1} as well as in the bending band ~1600 cm^{-1} (Fig. 3a and b). This initial increase occurs mostly within 20 minutes after hydration starts, which suggests that it may relate to initial water intrusion. About 6 h after hydration start, the hydrophobic reference deviates from this scheme and a predominant dip occurs in the stretching band at around 3050 cm^{-1} as well as a peakshift (from 1641 cm^{-1} to 1660 cm^{-1}) in the bending region, indicating that the water somewhere in the detection volume enhances its coordination in this process. The coincidence of these findings suggests that water diffusing into the more hydrophobic matrix preferentially coordinates with matrix silanol groups, which then partially deprotonate as the consequence. Proton conductivity along fine nanochannels of silanol-coordinated water [77,78] could explain the sudden occurrence of the dip by a percolation phenomenon that sets in after about 6 hours. This is also consistent with the relative change of the integral silanol signal displayed in Fig. 2d. Although the loss of silanol signal occurs nanometers below the surface, this very process seems to have a reordering effect on the molecular orientation of interfacial water

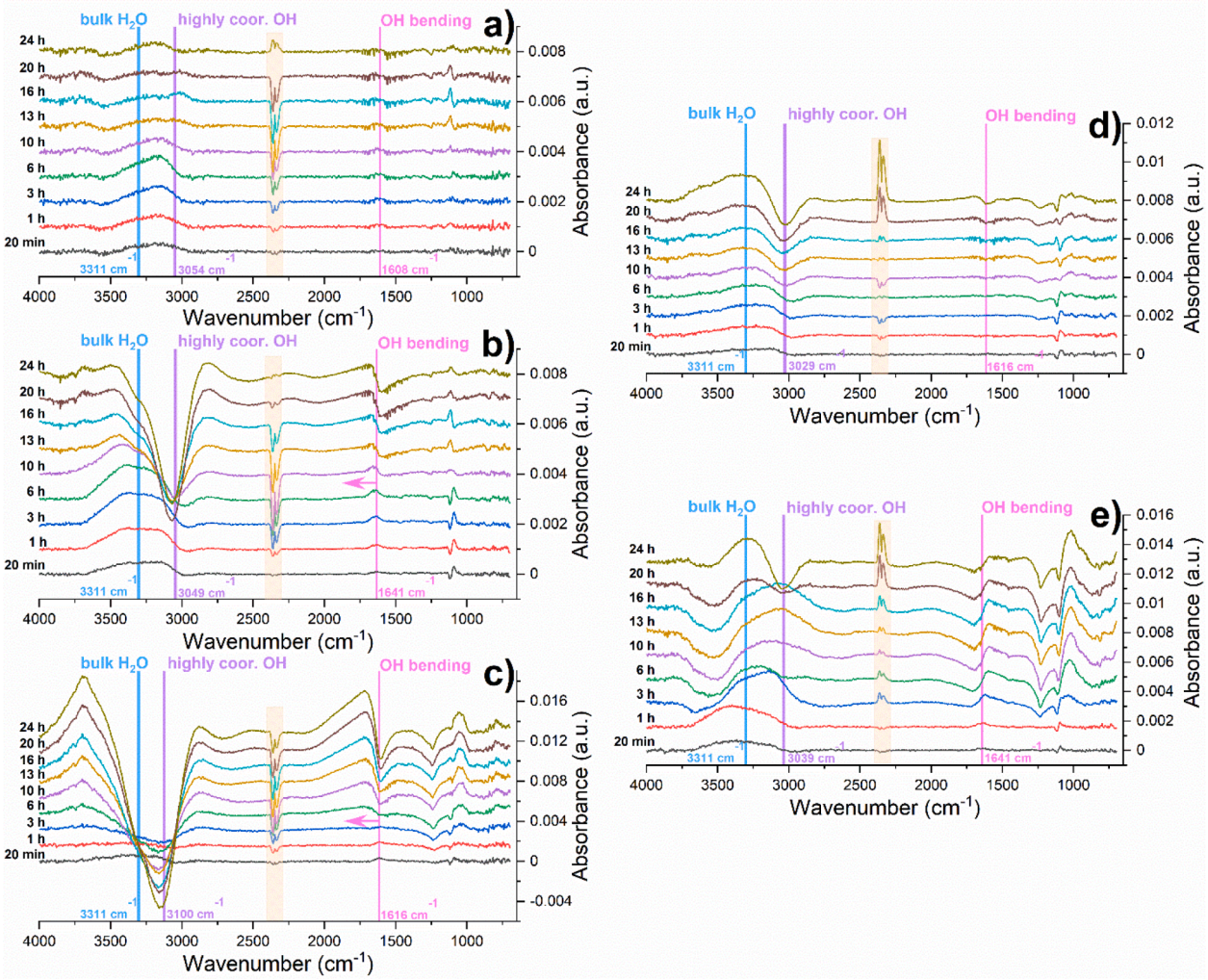

Fig. 3. Differential SEIRA spectra of a 24 h hydration series of 10 nm thick PPFs. **a)** SiOx film, **b)** SiO:CH film, **c)** Vgrad architecture (4 nm SiO:CH on 6 nm SiOx), **d)** Vgrad-ox1, and **e)** Vgrad-ox5. The spectra are shifted vertically by a factor of 10^{-3} each; the time series includes measurements at 20 min, 1 h, 3 h, 6 h, 10 h, 13 h, 16 h, 20 h, and 24 h after injection of water. The here presented spectra reveal the differences in the spectrum relative to the hydration start; vertical lines mark the peak positions of bulk water (blue line - at 3311 cm^{-1}), highly coordinated OH (purple line - at 3054, 3049, 3100, 3029, and 3039 cm^{-1} for SiOx, SiO:CH, Vgrad, Vgrad-ox1, and Vgrad-ox5, respectively) and OH bending vibration (pink line - at 1608, 1641, 1616, 1616, and 1641 cm^{-1} for SiOx, SiO:CH, Vgrad, Vgrad-ox1, and Vgrad-ox5, respectively). The orange shaded area marks the CO_2 absorption.

as discussed above (Fig. 2a), likely occurring around the defect spots at the surface that can be understood as an entrance for the nanochannels. The range of the underlying interaction must be long-range. Hydration thus proceeds in rather different ways depending on the type of matrix in these plain reference PPFs.

Fig. 3c further shows that similar mechanisms are at play in the composite Vgrad sample, albeit at relatively higher extent. The position of the differential dip in the OH stretching band of Vgrad (Fig. 3c) is located at exactly the same location as the dip of the SiO:CH reference film and must thus be of identical origin. The relative size of the differential dips is consistent with the integral envelopes analyzed above (viz. Fig. 2c and d). This amplification in Vgrad is somewhat surprising since the silanol rich SiO:CH terminal layer represents only ~40% of the film architecture, as compared to the plain SiO:CH reference layer. It is however in agreement with previous ToF-SIMS results suggesting a significantly elevated silanol content in the terminal layer of gradient architectures [22]. We believe that the in-situ change of plasma conditions (oxygen flow and energy) at the gradient during deposition entails a unique silanol density in the SiO:CH / SiOx gradient region of this type of architecture, likely by incorporation of trapped radicals in the graded plasma polymer transition region. We also note that the differential peakshift of the bending band is more pronounced for Vgrad (Fig. 3b) as

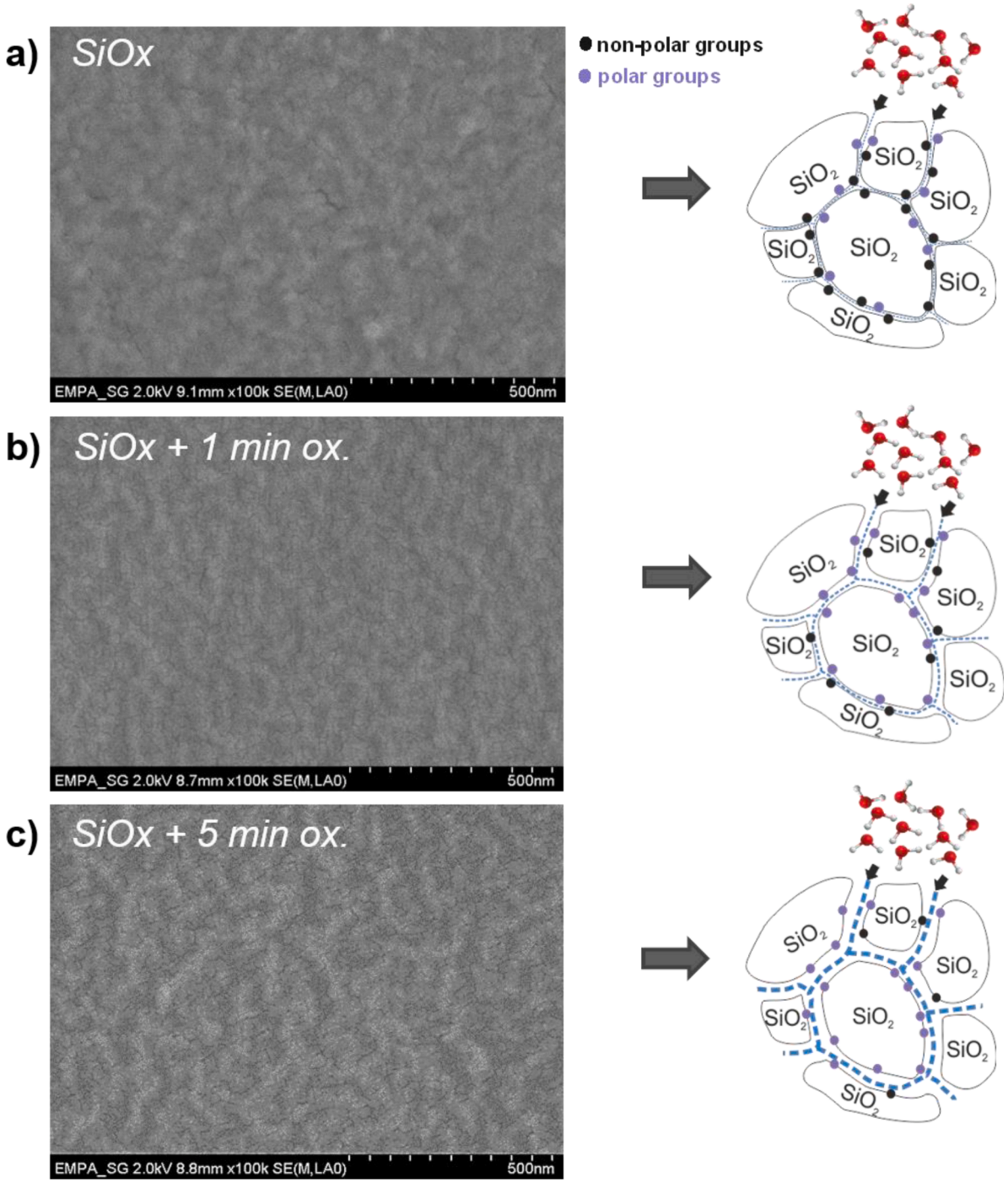

Fig. 4. SEM images of **a)** SiOx base layer, **b)** SiOx base layer after 1 min Ar/O_2 plasma etching, and **c)** SiOx base layer after 5 min Ar/O_2 plasma etching (all 6 nm thick; w/o cover layer). A granular structure is defined by linear, branched nanopores that increase in number and length with increasing Ar/O_2 etching time. The sketches illustrate how an increasing amount of water can penetrate into the pores during hydration.

compared to SiO:CH (Fig. 3c); this suggests that the interaction energetics of interfacial water is more strongly affected in the Vgrad architecture. Such energetic shifts are possibly linked to the occurrence of a long-range dipolar field that acts to reorientate interfacial water towards the horizontal plane (Fig. 1c). Comparing this result with the integral reduction of oriented water signal (Fig. 2c) we can recap that the Vgrad architecture has a strong and localized coordination effect on diffusing water molecules via silanol groups. The deprotonated silanol groups are able to affect the rotational orientation (i.e. libration) of water [79]. It is interesting to note that the energetic changes of the Vgrad bending band reach out into the libration combinatorial band of water around 2100 cm^{-1}. It would therefore be interesting for future work to study the water libration bands around 670 cm^{-1},particularly for the hydrated Vgrad architecture [50]. A change of water libration in the sense of a preferred orientation would have an increasing effect on the range of dipolar interactions with water. In addition, the Si-O-Si network modes belonging to the plasma polymer backbone around ~1100 cm^{-1}[29] are also enhanced during this reactive hydration process that eventually leads to silanol deprotonation.

The gradient structures with intermediate oxidation steps Vgrad-ox1 and Vgrad-ox5 exhibit a reduced differential dip in the OH stretching region (Fig. 3d and e). The plasma oxidation creates a nanoporous SiO_2-like matrix, showing increasing open structure with oxidation time. From previous ToF-SIMS measurements, we know, however, that the overall silanol content in the cover layer of intermediately oxidized gradients is comparable to the Vgrad sample [22], hence, we can also expect deprotonation effects. The large integral gain of water signal of the Vgrad-ox5 samples seen in Fig. 2c and also in the differential stretching band of Fig. 3e is remarkable. This evolution is not restricted to OH vibrations as can be seen from a significant reorganization in the Si-O-Si network modes around ~1100 cm^{-1}.

The intermediately oxidized gradient architectures seem to behave fundamentally differently from the Vgrad type architecture. In this context, it is interesting to note that there are important morphological changes occurring on the surface of the SiOx base layer during intermediate Ar/O_2 plasma etching as illustrated by the SEM images shown in Fig. 4. While the long-range surface roughness remains unaffected, defects (caused by the incorporated hydrocarbon fraction and trapped radicals) along the granule boundaries are starting points to open up a network of linear pores at the intersection of the boundaries during oxygen etching. This porous structure becomes visible by etching of the polymer substrate (so-called undercutting) [76,80]. Mainly, the pore volume of the 5 minutes oxidized PPF is clearly enhanced, i.e. longer and wider pores – seen as a branched network of fine dark lines. The hydration of these pores in the base layer would entrain larger amounts of water and create an exponentially amplified SEIRAS signal due to its relatively higher proximity near the Au plasmonic layer.

The intermediate Ar/O_2 etching has a profound effect on the morphology and chemical composition of the gradient architectures. A modified composition hence leads to significant differences in the evolution of the hydration process both chemically and physically. Intermediately oxidized gradients thus represent a new class of gradient architectures rather than a modified gradient.

Conclusion

This surface-enhanced IR absorption spectroscopy (SEIRAS) study of plain and graded plasma polymer films demonstrates how chemical and morphological details of the plasma polymer matrix, such as silanol group coordination and nanoporosity, affect interfacial water on remarkably long time scales of 24 hours after immersion in water. We found evidence that the vertically oriented portion of water at the aqueous interface is reduced in presence of a hydrophobic PPF surface (SiO:CH); this effect concurs with a rather sudden onset of deprotonation (i.e. percolation of hydrated nanochannels) of matrix silanol groups. These events are driven by a slow reactive diffusion process of water into the matrix and occur only after ~6 hours – several nanometers below the surface. The architecture of a 4 nm hydrophobic cover layer, deposited in situ on a 6 nm hydrophilic base layer (Vgrad) entails particularly strong effects in terms of interfacial water reorientation and strong physico-chemical water-matrix coordination, probably also affecting confined water libration and the ensuing range of dipolar interactions.

An intermediate Ar/O_2 etching of the 6 nm thick base layer leads to the occurrence and widening of pores; the mechanisms of loss of silanol matrix signal and interfacial reorientation are both significantly reduced by the Ar/O_2 etching. Moreover, excessive oxidation of 5 minutes leads to a pronounced nanoporous structure that can entrain significantly higher amounts of water during hydration, which seems to be accompanied by chemical rearrangements in the Si-O-Si network.

Declaration of Competing Interest

The authors declare that they have no known competing financial interests or personal relationships that could have appeared to influence the work reported in this paper.

Acknowledgments

We would like to acknowledge financial support by the Swiss National Science Foundation (SNSF project no. 200021_169180), as well as useful scientific discussion with Dr. Patrick Rupper and Dr. Sandra Gaiser at Empa. Joachim Heberle acknowledges funding by the Deutsche Forschungsgemeinschaft (SFB 1349 Project no. 387284271, project C5).

Supplementary materials

Supplementary material associated with this article can be found, in the online version, at doi:10.1016/j.surfin.2020.100922.

References

[1] A. Nilsson, L.G.M. Pettersson, The structural origin of anomalous properties of liquid water, Nature Comm. 6 (2015) 8998.
[2] V. Crupi, S. Interdonato, F. Longo, D. Majolino, P. Migliardo, V. Venuti, A new insight on the hydrogen bonding structures of nanoconfined water: a Raman study, J. Raman Spectrosc. 39 (2008) 244–249.
[3] D. Eisenberg, W. Kauzmann. The structure and properties of water, Oxford University Press, 2005.
[4] L.D. Gelb, K. Gubbins, R. Radhakrishnan, M. Sliwinska-Bartkowiak, Phase separation in confined systems, Rep. Progress Phys. 62 (1999) 1573.
[5] N. Nandi, B. Bagchi, Dielectric relaxation of biological water, J. Phys. Chem. B 101 (1997) 10954–10961.
[6] N.E. Levinger, Water in confinement, Science 298 (2002) 1722–1723.
[7] I.C. Bourg, C.I. Steefel, Molecular dynamics simulations of water structure and diffusion in silica nanopores, J. Phys. Chem. C 116 (2012) 11556–11564.
[8] P. Ball, Water as an active constituent in cell biology, Chem. Rev. 108 (2008) 74–108.
[9] G.W. Scherer, Crystallization in pores, Cement and Concrete Res. 29 (1999) 1347–1358.
[10] A. Verdaguer, G. Sacha, H. Bluhm, M. Salmeron, Molecular structure of water at interfaces: Wetting at the nanometer scale, Chem. Rev. 106 (2006) 1478–1510.
[11] S. Mani, F. Khabaz, R.V. Godbole, R.C. Hedden, R. Khare, Structure and hydrogen bonding of water in polyacrylate gels: effects of polymer hydrophilicity and water concentration, J. Phys. Chem. B 119 (2015) 15381–15393.
[12] E. Spohr, A. Trokhymchuk, D. Henderson, Adsorption of water molecules in slit pores, J. Electroanal. Chem. 450 (1998) 281–287.
[13] P.A. Bonnaud, B. Coasne, R.J. Pellenq, Molecular simulation of water confined in nanoporous silica, J. Phys. Condens. Matter 22 (2010), 284110.
[14] D. Argyris, D.R. Cole, A. Striolo, Hydration structure on crystalline silica substrates, Langmuir 25 (2009) 8025–8035.
[15] S. Romero-Vargas Castrillón, N. Giovambattista, I.A. Aksay, P.G. Debenedetti, Evolution from surface-influenced to bulk-like dynamics in nanoscopically confined water, J. Phys. Chem. B 113 (2009) 7973–7976.
[16] J. Puibasset, R.J. Pellenq, A grand canonical Monte Carlo simulation study of water adsorption on Vycor-like hydrophilic mesoporous silica at different temperatures, J. Phys. Condens. Matter 16 (2004) S5329.
[17] J. Zanotti, M. Bellissent-Funel, S. Chen, A. Kolesnikov, Further evidence of a liquid–liquid transition in interfacial water, J. Phys. Condens. Matter 18 (2006) S2299.

[18] V.F. Tarasov, S.D. Chemerisov, A.D. Trifunac, H-atom electron-spin polarization in irradiated water and ice confined in the nanopores of Vycor glass, J. Phys. Chem. B 107 (2003) 1293–1301.
[19] Y. Zhou, B. Josey, E. Anim-Danso, B. Maranville, J. Karapetrova, Z. Jiang, Q. Zhou, A. Dhinojwala, M.D. Foster, In situ nanoscale characterization of water penetration through plasma polymerized coatings, Langmuir 34 (2018) 9634–9644.
[20] V. Purohit, E. Mielczarski, J.A. Mielczarski, L. Akesso, Evidence of coexistence of micro and nanoporosity of organo-silica polymeric films deposited on silicon by plasma deposition, Mater. Chem. Phys. 141 (2013) 602–612.
[21] M. Jaritz, C. Hopmann, S. Wilski, L. Kleines, M. Rudolph, P. Awakowicz, R. Dahlmann, HMDSO-based thin plasma polymers as corrosion barrier against NaOH solution, J. Mater. Eng. Perform. (2020) 1–9.
[22] E. Bülbül, P. Rupper, T. Geue, L. Bernard, M. Heuberger, D. Hegemann, Extending the range of controlling protein adsorption via subsurface architecture, ACS Appl. Mater. Interfac. 11 (2019) 42760–42772.
[23] E. Bülbül, D. Hegemann, T. Geue, M. Heuberger, How the dynamics of subsurface hydration regulates protein-surface interactions, Colloids and Surfaces B: Biointerfaces 190 (2020), 110908.
[24] D. Hegemann, N. Hocquard, M. Heuberger, Nanoconfined water can orient and cause long-range dipolar interactions with biomolecules, Sci. Rep. 7 (2017) 17852.
[25] D. Hegemann, N.E. Blanchard, M. Heuberger, Reduced protein adsorption on plasma polymer films comprising hydrophobic/hydrophilic vertical chemical gradients, Plasma Processes and Polymers 13 (2016) 494–498.
[26] D. Hegemann, E. Bülbül, B. Hanselmann, U. Schütz, M. Amberg, S. Gaiser, Plasma polymerization of hexamethyldisiloxane: Revisited, Plasma Processes and Polymers 18 (2021), e2000176.
[27] L. Dalstein, E. Potapova, E. Tyrode, The elusive silica/water interface: Isolated silanols under water as revealed by vibrational sum frequency spectroscopy, Phys. Chem. Chem. Phys. 19 (2017) 10343–10349.
[28] K.S. Smirnov, Structure and sum-frequency generation spectra of water on uncharged Q 4 silica surfaces: a molecular dynamics study, Phys. Chem. Chem. Phys. 22 (2020) 2033–2045.
[29] S.L. Warring, D.A. Beattie, A.J. McQuillan, Surficial siloxane-to-silanol interconversion during room-temperature hydration/dehydration of amorphous silica films observed by ATR-IR and TIR-raman spectroscopy, Langmuir 32 (2016) 1568–1576.
[30] T.A. Michalske, S.W. Freiman, A molecular interpretation of stress corrosion in silica, Nature 295 (1982) 511–512.
[31] D. Ngo, H. Liu, Z. Chen, H. Kaya, T.J. Zimudzi, S. Gin, T. Mahadevan, J. Du, S. H. Kim, Hydrogen bonding interactions of H 2 O and SiOH on a boroaluminosilicate glass corroded in aqueous solution, NPJ Mater. Degrad. 4 (2020) 1–14.
[32] A. Anderson, W.R. Ashurst, Interfacial water structure on a highly hydroxylated silica film, Langmuir 25 (2009) 11549–11554.
[33] M. Yalamanchili, A. Atia, J. Miller, Analysis of interfacial water at a hydrophilic silicon surface by in-situ FTIR/internal reflection spectroscopy, Langmuir 12 (1996) 4176–4184.
[34] J. Kiefer, K. Frank, F.M. Zehentbauer, H.P. Schuchmann, Infrared spectroscopy of bilberry extract water-in-oil emulsions: sensing the water-oil interface, Biosensors 6 (2016) 13.
[35] L. Scatena, M. Brown, G. Richmond, Water at hydrophobic surfaces: Weak hydrogen bonding and strong orientation effects, Science 292 (2001) 908–912.
[36] K.C. Jena, D.K. Hore, Water structure at solid surfaces and its implications for biomolecule adsorption, Phys. Chem. Chem. Phys. 12 (2010) 14383–14404.
[37] A.L. Barnette, D.B. Asay, S.H. Kim, Average molecular orientations in the adsorbed water layers on silicon oxide in ambient conditions, Phys. Chem. Chem. Phys. 10 (2008) 4981–4986.
[38] T. Petit, L. Puskar, T. Dolenko, S. Choudhury, E. Ritter, S. Burikov, K. Laptinskiy, Q. Brzustowski, U. Schade, H. Yuzawa, Unusual water hydrogen bond network around hydrogenated nanodiamonds, J. Phys. Chem. C 121 (2017) 5185–5194.
[39] G. Nikolic, D. Cvetkovic, M. Cakic. Fourier Transforms: High-tech Application and Current Trends, Intech Open, 2017.
[40] G.E. Ewing, Thin film water, ACS Publications, 2004.
[41] Q. Du, E. Freysz, Y.R. Shen, Surface vibrational spectroscopic studies of hydrogen bonding and hydrophobicity, Science 264 (1994) 826–828.
[42] F.H. Stillinger, T.A. Weber, Inherent structure in water, J. Phys. Chem. 87 (1983) 2833–2840.
[43] A. Poda, A. Anderson, W. Ashurst, Self-assembled octadecyltrichlorosilane monolayer formation on a highly hydrated silica film, Appl. Surf. Sci. 256 (2010) 6805–6813.
[44] A.-M. Putz, M.V. Putz, Spectral inverse quantum (Spectral-IQ) method for modeling mesoporous systems: Application on silica films by FTIR, Int. J. Mol. Sci. 13 (2012) 15925–15941.
[45] A. Striolo, Understanding interfacial water and its role in practical applications using molecular simulations, MRS Bull. 39 (2014) 1062–1067.
[46] S.E. Sanders, P.B. Petersen, Heterodyne-detected sum frequency generation of water at surfaces with varying hydrophobicity, J. Chem. Phys. 150 (2019), 204708.
[47] L. Chen, X. He, H. Liu, L. Qian, S.H. Kim, Water adsorption on hydrophilic and hydrophobic surfaces of silicon, J. Phys. Chem. C 122 (2018) 11385–11391.
[48] A.B. McCoy, The role of electrical anharmonicity in the association band in the water spectrum, J. Phys. Chem. B 118 (2014) 8286–8294.
[49] P.K. Verma, A. Kundu, M.S. Puretz, C. Dhoonmoon, O.S. Chegwidden, C. H. Londergan, M. Cho, The bend+ libration combination band is an intrinsic, collective, and strongly solute-dependent reporter on the hydrogen bonding network of liquid water, J. Phys. Chem. B 122 (2017) 2587–2599.
[50] Y. Tong, T. Kampfrath, R.K. Campen, Experimentally probing the libration of interfacial water: the rotational potential of water is stiffer at the air/water interface than in bulk liquid, Phys. Chem. Chem. Phys. 18 (2016) 18424–18430.
[51] M. Prasad, N.J. English, S.Nath Chakraborty, Relaxation dynamics and power spectra of liquid water: a molecular dynamics simulation study, Mol. Phys. (2020) 1–9.
[52] M. Grossutti, J.J. Leitch, R. Seenath, M. Karaskiewicz, J. Lipkowski, SEIRAS studies of water structure in a sodium dodecyl sulfate film adsorbed at a gold electrode surface, Langmuir 31 (2015) 4411–4418.
[53] M. Dunwell, Y. Yan, B. Xu, A surface-enhanced infrared absorption spectroscopic study of pH dependent water adsorption on Au, Surf. Sci. 650 (2016) 51–56.
[54] T. Uchida, M. Osawa, J. Lipkowski, SEIRAS studies of water structure at the gold electrode surface in the presence of supported lipid bilayer, J. Electroanal. Chem. 716 (2014) 112–119.
[55] Z. Su, J. Juhaniewicz-Debinska, S. Sek, J. Lipkowski, Water structure in the submembrane region of a floating lipid bilayer: the effect of an ion channel formation and the channel blocker, Langmuir 36 (2019) 409–418.
[56] Surface-Enhanced Infrared Absorption M. Osawa, Surface-Enhanced Infrared Absorption, in: S. Kawata (Ed.), Springer Berlin Heidelberg, Berlin, Heidelberg, 2001, pp. 163–187.
[57] M. Osawa, K.-I. Ataka, K. Yoshii, Y. Nishikawa, Surface-enhanced infrared spectroscopy: the origin of the absorption enhancement and band selection rule in the infrared spectra of molecules adsorbed on fine metal particles, Appl. Spectros. 47 (1993) 1497–1502.
[58] X. Jiang, E. Zaitseva, M. Schmidt, F. Siebert, M. Engelhard, R. Schlesinger, K. Ataka, R. Vogel, J. Heberle, Resolving voltage-dependent structural changes of a membrane photoreceptor by surface-enhanced IR difference spectroscopy, Proc. Natl. Acad. Sci. 105 (2008) 12113–12117.
[59] K. Ataka, S.T. Stripp, J. Heberle, Surface-enhanced infrared absorption spectroscopy (SEIRAS) to probe monolayers of membrane proteins, Biochimica et Biophysica Acta (BBA)-Biomembranes 1828 (2013) 2283–2293.
[60] K. Ataka, J. Heberle, Biochemical applications of surface-enhanced infrared absorption spectroscopy, Anal. Bioanal. Chem. 388 (2007) 47–54.
[61] K.-I. Ataka, M. Osawa, In situ infrared study of water− sulfate coadsorption on gold (111) in sulfuric acid solutions, Langmuir 14 (1998) 951–959.
[62] Z. Zhang, T. Imae, Study of surface-enhanced infrared spectroscopy: 1. Dependence of the enhancement on thickness of metal island films and structure of chemisorbed molecules, J. Colloid and Interface Sci. 233 (2001) 99–106.
[63] K. Ataka, J. Heberle, Use of surface enhanced infrared absorption spectroscopy (SEIRA) to probe the functionality of a protein monolayer, Biopolym. Orig. Res. Biomol. 82 (2006) 415–419.
[64] S.K. Rutledge, J.A. Mihelcic, Undercutting of defects in thin film protective coatings on polymer surfaces exposed to atomic oxygen, Surf. Coat. Tech. 39 (1989) 607–615.
[65] F. Mitschker, S. Steves, M. Gebhard, M. Rudolph, L. Schücke, D. Kirchheim, M. Jaritz, M. Brochhagen, C. Hoppe, R. Dahlmann, Influence of PE-CVD and PE-ALD on defect formation in permeation barrier films on PET and correlation to atomic oxygen fluence, J. Phys. D Appl. Phys. 50 (2017), 235201.
[66] P. Raynaud, B. Despax, Y. Segui, H. Caquineau, FTIR plasma phase analysis of hexamethyldisiloxane discharge in microwave multipolar plasma at different electrical powers, Plasma Processes and Polymers 2 (2005) 45–52.
[67] N.E. Blanchard, V.V. Naik, T. Geue, O. Kahle, D. Hegemann, M. Heuberger, Response of plasma-polymerized hexamethyldisiloxane films to aqueous environments, Langmuir 31 (2015) 12944–12953.
[68] M. Gierada, I. Petit, J. Handzlik, F. Tielens, Hydration in silica based mesoporous materials: a DFT model, Phys. Chem. Chem. Phys. 18 (2016) 32962–32972.
[69] M.G. Bridelli. Fourier transform infrared spectroscopy in the study of hydrated biological macromolecules, Fourier Transforms-High-tech Application and Current Trends, InTech, Rijeka, 2017, pp. 191–213.
[70] J. Paul, R. Provencal, C. Chapo, K. Roth, R. Casaes, R. Saykally, Infrared cavity ringdown spectroscopy of the water cluster bending vibrations, J. Phys. Chem. A 103 (1999) 2972–2974.
[71] I.-S. Chuang, G.E. Maciel, A detailed model of local structure and silanol hydrogen bonding of silica gel surfaces, J. Phys. Chem. B 101 (1997) 3052–3064.
[72] E. Bonnell, L. Yu, D. Homa, G. Pickrell, A. Wang, Temperature dependent behavior of optical loss from hydrogen species in optical fibers, Micro-and Nanotechnology Sensors, Systems, and Applications VII, Int. Soc. Opt. Photon. (2015) 94671L.
[73] M.A. Brook, Silicon in organic, organometallic, and polymer chemistry, Wiley, New York, 2000.
[74] D. Muñoz-Santiburcio, D. Marx, Nanoconfinement in slit pores enhances water self-dissociation, Phys. Rev. Lett. 119 (2017), 056002.
[75] S. Ruiz-Barragan, D. Muñoz-Santiburcio, D. Marx, Nanoconfined water within graphene slit pores adopts distinct confinement-dependent regimes, J. Phys. Chem. Lett. 10 (2018) 329–334.
[76] A. Erlat, R. Spontak, R. Clarke, T. Robinson, P. Haaland, Y. Tropsha, N. Harvey, E. Vogler, SiOx gas barrier coatings on polymer substrates: morphology and gas transport considerations, J. Phys. Chem. B 103 (1999) 6047–6055.
[77] J. Guo, X.-Z. Li, J. Peng, E.-G. Wang, Y. Jiang, Atomic-scale investigation of nuclear quantum effects of surface water: Experiments and theory, Progress Surf. Sci. 92 (2017) 203–239.
[78] G. Reiter, C. Burnham, D. Homouz, P. Platzman, J. Mayers, T. Abdul-Redah, A. Moravsky, J. Li, C.-K. Loong, A. Kolesnikov, Anomalous behavior of proton zero

point motion in water confined in carbon nanotubes, Phys. Rev. Lett. 97 (2006), 247801.
[79] R. Renou, A. Szymczyk, A. Ghoufi, Water confinement in nanoporous silica materials, J. Chem. Phys. 140 (2014), 044704.
[80] J. Yun, S. Lee, Y. Jeong, H.-R. Lee, J.-D. Kwon, G.-H. Lee, Reduction of defects in SiOx vapor permeation barriers on polymer substrates by introducing a sputtered interlayer, Jpn. J. Appl. Phys. 48 (2009), 055503.